

Transverse Dynamics and Energy Tuning of Fast Electrons
Generated in Sub-Relativistic Intensity Laser Pulse Interaction
with Plasmas

Michiaki Mori, Masaki Kando, Izuru Daito, Hideyuki Kotaki, Yukio
Hayashi, Atsushi Yamazaki, Koichi Ogura, Akito Sagisaka, James Koga,
Kazuhisa Nakajima, Hiroyuki Daido, Sergei V. Bulanov, and Toyoaki Kimura
Advanced Photon Research Center, Japan Atomic Energy Agency,
Umemidai 8-1, Kizu, Kyoto, 619-0215 Japan

(Dated: March 31, 2022)

Abstract

The regimes of quasi-mono-energetic electron beam generation were experimentally studied in the sub-relativistic intensity laser plasma interaction. The observed electron acceleration regime is unfolded with two-dimensional-particle-in-cell simulations of laser-wake field generation in the self-modulation regime.

E-mail: morimichiaki@jaea.go.jp

I. INTRODUCTION

Laser accelerator [1] development is now entering a new mature stage in which it has become possible to manipulate in a controllable way the parameters of accelerated charged particle beams. For a broad range of applications, high stability in ultrarelativistic electron production is required, which implies high directionality, controllability and reproducibility in the accelerated electron energy and collimation. Quasi-monoenergetic electron beam generation has been observed in several laser-plasma interaction experiments, the results of which are presented in Refs. [2, 3]. This breakthrough resulted from many previous investigations of laser-driven charged particle acceleration conducted by a number of scientific groups (see Ref. [4]), where the high energy electron production and huge accelerating gradients (~ 100 GV/m) have been observed.

In a majority of the above mentioned experiments, the intensity of the laser light at the focus was relativistic, i.e. the dimensionless laser field amplitude, $a_0 = eE_0/m_e\omega c$, was greater than unity: $a_0 \approx 0.85[(I=10^{18} \text{ W/cm}^2)(\lambda=1 \text{ }\mu\text{m})^2]^{1/2} > 1$. Here, e is the electron charge, E_0 is the laser pulse peak electric field, m_e is the electron mass, ω is the laser frequency, and c is the speed of light in vacuum. Moreover, the plasma density was also substantially large, e.g. the electron density at which the quasi-monoenergetic electron production was observed [2, 3], ranged from $6 \cdot 10^{18} \text{ cm}^{-3}$ to $1.3 \cdot 10^{20} \text{ cm}^{-3}$. High enough electron density provides favorable conditions for self-focusing and stimulated Raman scattering development resulting in laser pulse self-modulation and the enhancement of the wake-field amplitude. This leads to the wake-wave-breaking and the electron injection into the acceleration phase. On the other hand the nonlinear process development raises additional questions on the directionality of the accelerated electron bunches, which demonstrates a need of further thorough experimental studies of the quasi-monoenergetic electron beam generation.

Below, in this letter, we present the results of experiments on the electron acceleration during a multi-terawatt femtosecond range laser interaction with an underdense plasma under the conditions, when the self-modulated wake-field regime occurs [5]. The acceleration regime is corroborated with 2D-particle-in-cell computer simulations of the laser pulse interaction with the underdense plasma.

II. EXPERIMENTAL SETUP AND CONDITION

The experiments are performed with a terawatt 10 Hz Ti:Sapphire CPA laser system "JLITE-X" ($\lambda = 800 \text{ nm}$) at the Advanced Photon Research Center of the Japan Atomic Energy Agency (JAEA-APRC). The laser pulse with 230 mJ pulse energy on target has a typical duration (half maximum) equal to 70 fs. The estimated peak power of the laser beam is 3 TW. The ratio of the prepulse to the main pulse intensity is less than 10^{-5} . The laser beam is focused onto the target by using a 15° , 646 mm focal length, $f/13$ θ -axis parabolic mirror. The spot size at the focus is 15 μm at half maximum and 25 μm at $1/e^2$. The energy concentration is 55 % within the $1/e^2$ spot. The focal peak intensity is estimated to be $9 \times 10^{17} \text{ W/cm}^2$. It corresponds to a dimensionless amplitude of the laser field, a_0 , equal to 0.67. By evacuating the laser beam path between the pulse compressor and the interaction chamber the pressure is made to be less than 10^{-1} Pa . We measured the neutral gas density in the target, a 600 μm long supersonic He gas-jet, by using a Mach-Zehnder interferometer. The plasma density is calculated by doubling the neutral gas density under the assumption of full helium ionization. This assumption is based on the fact that for our experimental conditions the barrier-suppression-ionization threshold intensity for He^{2+} is equal to $3.9 \times 10^{16} \text{ W/cm}^2$ [6] and the tunneling ionization threshold is $8.8 \times 10^{15} \text{ W/cm}^2$. These thresholds are well below the laser intensity at focus, 10^{18} W/cm^2 . As a result the plasma density at the focus is calculated to be $n_0 = 5 \times 10^{19} \text{ cm}^{-3}$. For the above parameters the wake wave wavelength, $\lambda_p = 2c/\omega_{pe} \approx 10 \mu\text{m}$, is shorter than the pulse length, which is about 30 μm . The laser power, 3 TW, is above the threshold for the relativistic self-focusing, $P > P_{cr} = 17(\omega_{pe}/c)^2 \text{ GW}$, [7]. Here $\omega_{pe} = (4\pi n_0 e^2/m_e)^{1/2}$ is the Langmuir frequency and λ_p is the laser wavelength.

In order to detect an energetic electron spectrum, we use an electron spectrometer (ESM) which is composed of a slit shape lead collimator (the slit width, w , is equal to 5 mm), an electromagnet, and two-layered Imaging Plates (IP) [BAS-SR, Fujifilm product]. The spectrometer is placed at the rear side of the target behind the interaction point. Each IP is covered with 12 μm thick Al foil in order to avoid exposure to visible light and the low energy electron component. We note that the IP is sensitive not only to the signal created by the fast electrons but also to the X-rays. As a consequence of this, there is a problem of separation of the signal produced by the electrons from the noise originating from the

X-rays. In order to obtain an IP image which is predominantly formed by the electron beam and to ascertain whether the electron beam contains a quasi-monoenergetic component, we varied the magnetic field value from 0 to 0.13 T by changing the drive electric current in the electromagnet. As a result, we found that X-ray signal effects are not so important for estimating the electron number.

III. EXPERIMENTAL RESULTS

Figure 1 shows the typical energy resolved electron beam image obtained with the ESM and the electron energy spectrum. Here, the horizontal coordinate presents the energy profile at the IP and the vertical coordinate shows the electron spatial distribution. The image is taken from a single shot. In this case, the plasma density is set to be $4.7 \times 10^{19} \text{ cm}^{-3}$. A well localized in space and energy spot is seen in the vicinity of the energy equal to 19.6 MeV. The image spatial size at the IP in the vertical direction is 5.7 mm at the half maximum. For the distance between the gas jet and the IP equal to 760 mm, we find the electron beam divergence to be about 7.5 mrad. We point out that for lower plasma density, $n = 3.1 \times 10^{19} \text{ cm}^{-3}$, the electron energy distribution taken with ten accumulated shots, does not show a high energy component in the electron beam. In order to obtain the electron number in the quasi-monoenergetic components, we integrate the electron distribution at the IP over the energy. By using the sensitivity of the IP (see Ref. [8]), the total charge of the quasi-monoenergetic electron component in the energy range from 16.3 to 25 MeV and in the angle 5 mrad is found to be 0.8 pC with the energy spread approximately equal to 4.8 MeV at the half maximum.

We have also observed spatial-spectral split images. The typical spatial (along the vertical axis) and spectral (along the horizontal axis) resolved images are shown in Fig. 2. These images are taken in a single shot under the same conditions as in the case presented in Fig. 1. In Fig. 2 (a), we see a single peak in space and a double peak in the energy distribution. The energies of the double peak component are 13.5 MeV and 18.1 MeV, respectively. In Fig. 2 (b), a triple spatial split peak with different quasi-monoenergetic energies is presented. Here, the peak energies of the triple peak are 3.3 MeV, 4.5 MeV, and 7.5 MeV, respectively. The directionality of electron beam with respect to the laser propagation direction are -13 mrad, 6 mrad, and 20 mrad.

We are able to control the electron beam parameters by changing the plasma density in the target. Figure 3 a) shows the electron energy spectra (each of them is taken in a single shot) at four different values of the plasma density. By increasing slightly the backing pressure of the gas jet the plasma density is set to be equal to $4.1 \cdot 10^{19} \text{ cm}^{-3}$ (1), $4.7 \cdot 10^{19} \text{ cm}^{-3}$ (2), $5.0 \cdot 10^{19} \text{ cm}^{-3}$ (3), and $6.6 \cdot 10^{19} \text{ cm}^{-3}$ (4). This results in changing the position of the quasi-monoenergetic peak from 8.5 MeV to 19.6 MeV. At the plasma density above $4.7 \cdot 10^{19} \text{ cm}^{-3}$, the energy width of the electron beam becomes broadened.

IV. RESULTS OF 2D-PIC SIMULATIONS

In order to elucidate the acceleration regime responsible for the quasi-monoenergetic electron beam formation, extensive two-dimensional PIC simulations of the laser pulse interaction with the underdense plasma target have been performed with the use of the REM P code [9]. In the simulations presented here a linearly p-polarized laser pulse with the dimensionless amplitude $a_0 = 0.67$, corresponding to the peak intensity $I = 9 \cdot 10^{17} \text{ W/cm}^2$ for $\lambda = 0.8 \text{ }\mu\text{m}$ laser, propagates along the x axis. The laser pulse has a Gaussian envelope with FWHM size $27 \cdot 31 \text{ }\mu\text{m}^2$. The plasma density is $n_0 = 2.32 \cdot 10^2 n_{cr}$, i.e. $n_0 = 5 \cdot 10^{19} \text{ cm}^{-3}$, which corresponds to $\beta_{pe} = 0.153$. Ions have an absolute charge two times larger than the electrons, and mass ratio $m_i = m_e \cdot 4 \cdot 1836$. The simulation box has $4500 \cdot 620$ grid points with a $0.1 \text{ }\mu\text{m}$ mesh size. The target has the form of an underdense plasma slab of size $425 \cdot 60 \text{ }\mu\text{m}^2$. The total number of quasiparticles is about 10^7 . The boundary conditions are absorbing in all directions for both the electromagnetic (EM) radiation and the quasiparticles. The space and time units are the wavelength and the period $2\pi = \omega$ of the incident radiation.

Under the conditions of simulations as in the case of the above discussed experiment the laser pulse length is approximately 4 times larger than the wake wavelength, $2\pi = \beta_{pe}$, and the observed laser pulse evolution corresponds to the development of the self-modulation regime. According to Ref. [5] in this regime the modulational instability results in the laser pulse modulations in the longitudinal direction and in the generation of the wake plasma wave in and behind the laser pulse. In Fig. 4 we present the electron density distribution in the (x;y) plane at $t = 300$, which shows a regular structure in the wake plasma wave left behind the laser pulse. The wake wave has a finite length, which corresponds to the finite time required

for the modulational instability development. In frame b) we plot the E_z component of the electric field along the laser pulse axis, $y = 0$, for $t = 300$. This clearly demonstrates that the initially Gaussian laser pulse becomes modulated with a modulation wavelength equal to the wake wave wavelength and its maximal amplitude becomes substantially higher, by a factor larger than 2, than the initial pulse amplitude. In frame c) we present the longitudinal, E_x , component of the electric field along the laser pulse axis, $y = 0$, for $t = 300$, which characterizes the evolution of the wake wave structure. We point out that the wake field has a regular structure behind the laser pulse over a distance substantially longer than the laser pulse length (see Fig. 4 c)).

The dependence of the electron energy spectrum on the target density found from the PIC simulations (see Fig. 3 b)) has a behavior similar to that in the experiment, which is seen in Fig. 3 (a). This clearly demonstrates the typicalness of the electron acceleration regime realized in the present work.

In Fig. 5, projections of the electron phase space, a) plane $(x;p_x)$, b) plane $(y;p_x)$, and c) plane $(x;p_y)$, at $t = 400$ are plotted. The transverse wake wave breaking of multiple wake cycles results in the electron injection into the acceleration phase with the production of multiple fast electron bunches seen in Fig. 5 a). At the time about $t = 400$ the electrons reach their maximal energy of the order of 30 MeV. The electrons with the maximal energy are accelerated in the 2-nd wake period, as seen in the electron phase plane, $(x;p_x)$, presented in Fig. 5 a). The electron injection occurs not in the first cycle of the wake wave according to the theory of the transverse wake wave breaking, which predicts that in a tenuous plasma the wake wave breaks at a finite distance behind the wake wave front, [10]. In Figs. 5 a) and c) we indicate by the dashed line the position of the laser pulse leading edge. It is at $x = 375$ and first electron bunch is localized at $x = 365$. The electron energy spectrum has the form of a quasi-monoenergetic bunch with a maximum at 20 MeV (see Fig. 3 b), and width $\sim 20\%$. The experimentally obtained form of the quasi-monoenergetic electron beam as seen in Fig. 1 is in good agreement with these results. Phase planes b) $(y;p_x)$ and c) $(x;p_y)$, show that spatially separated bunches are accelerated in subsequent wake wave periods. In the frames a) and b) the arrows A and B indicate the spatially separated electron beamlets, which also have different energies. In the $(x;p_y)$ phase plane c), arrows indicate the aside beamlets. Inside the 2-nd wake period, a quasi-monoenergetic electron bunch with its energy of about 20 MeV is generated (indicated by the arrow A).

In addition, broadened quasi-monoenergetic electron bunches with energy approximately equal to 10 MeV can be seen in the 2nd and 3rd wake periods (indicated by the arrow B). These features are in sufficiently good agreement with the multiple quasi-monoenergetic electron beam production observed in our experiments and shown in Fig. 2 (a). In addition, 2D-PIC simulations also demonstrate the bending of electron beam bunches. The transverse electron momentum versus the x-coordinate is shown in Fig. 5 (c). We can see that the electron bunches in the 3rd wake period have finite transverse momentum beams (indicated by the arrows) and have the y-component of their momentum equal to approximately 4. This corresponds to the generic property of the wakefield acceleration, when the electron is trapped both in the longitudinal and transverse directions. According to Ref. [1] the characteristic time scale of the electron longitudinal motion is equal to the acceleration time, $t_{acc} = \frac{1}{\omega_{pe}} \frac{2}{\omega_{ph}}$. Here $\omega_{ph} = \omega_{pe} \frac{1}{\gamma}$ is the gamma factor associated with the wake wave phase velocity, v_{ph} , i.e. $\omega_{ph} = \omega_{pe} \frac{1}{\sqrt{1 - (v_{ph}/c)^2}}$ (see for details review article [11] and quoted literature). In the transverse direction, the electrons being injected with a finite transverse momentum (see Refs. [10, 12]), move along a wiggling trajectory, also called betatron oscillations, in which the frequency and amplitude change, with a typical time scale given by $t_b = \frac{1}{\omega_{pe}} \frac{1}{\gamma_e^2}$ [13], where γ_e is the fast electron relativistic gamma factor. We point out that the beam transverse dynamics determines its transverse emittance (e.g. see Ref. [14]). From the 2D-PIC simulation results, presented in Fig. 5, the electron beam divergence is estimated to be in the range from 10 to 20 mrad, which is in sufficiently good agreement with the experimental data as seen in Fig. 2 (b).

V. SUMMARY

In conclusion, when a 3 TW laser beam with a pulse duration equal to 70 fs is focused by a f/130 Axis-Parabolic mirror into a He gas jet target of length 600 μ m, the quasi-monoenergetic electron beams are observed. By changing the target plasma density the fast electron energy and their energy spectrum change in a controllable way. The 2D-PIC simulations demonstrate that the wakefield generation occurs in the self-modulated laser wakefield acceleration regime when multiple fast electron bunch generation occurs and the bunches are well localized both in energy and coordinate space. The PIC simulations qualitatively reproduce the dependence of the experimentally observed energy spectrum on

the plasma density.

Acknowledgements

We acknowledge Prof. T. Tajima for fruitful discussions and Dr. T. Zh. Esirkepov for providing the 2D-PIC simulation code. This work was partly supported by the Ministry of Education, Culture, Sports, Science and Technology of Japan, Grant-Aid for Specially Promoted Research No. 15002013.

-
- [1] T. Tajima and J.M. Dawson, *Phys. Rev. Lett.* 43 (1979) 267.
 - [2] S.P.D. Mangles et al., *Nature* 431 (2004) 535; C.G.R. Geddes et al., *Nature* 431 (2004) 538; J. Faure et al., *Nature* 431 (2004) 541.
 - [3] E. Mura et al., *Appl. Phys. Lett.* 86 (2005) 251501; A. Yamazaki et al., *Phys. Plasmas* 12 (2005) 093101.
 - [4] Y. Kitagawa et al., *Phys. Rev. Lett.* 68 (1992) 48; C.E. Clayton et al., *Phys. Rev. Lett.* 70 (1993) 37; K. Naka-jima et al., *Phys. Rev. Lett.* 74 (1995) 4428; A. Modena et al., *Nature* 377 (1995) 606; D. Umstadter et al., *Science* 273 (1996) 472; F. Amirano et al., *Phys. Rev. Lett.* 81 (1998) 995; V. Malka et al., *Science* 298 (2002) 1600.
 - [5] P. Sprangle et al., *Phys. Rev. Lett.* 69 (1992) 2200; N.E. Andreev et al., *JETP Lett.* 55 (1992) 571; T.M. Antonsen, Jr., and P. Mora, *Phys. Rev. Lett.* 69 (1992) 2204.
 - [6] S. August et al., *Phys. Rev. Lett.* 63 (1989) 2212.
 - [7] G.Z. Sun et al., *Phys. Fluids* 30 (1987) 526; D. Bames, T. Kurki-Suonio and T. Tajima, *IEEE Trans. Plasma Sci.* PS-15 (1987) 154.
 - [8] K.A. Tanaka et al., *Rev. Sci. Inst.* 76 (2005) 013507.
 - [9] T. Zh. Esirkepov, *Comput. Phys. Commun.* 135 (2001) 144.
 - [10] S.V. Bulanov et al., *Phys. Rev. Lett.* 78 (1997) 4205; T.V. Liseikina et al., *Phys. Rev. E* 60 (1999) 5991.
 - [11] G. Mourou, T. Tajima and S.V. Bulanov, *Rev. Mod. Phys.* 78 (2006) (in press).
 - [12] A. Pukhov and J. Meyer-ter-Vehn, *Appl. Phys. B* 74 (2002) 355; H. Xu et al., *Phys. Plasmas* 12 (2005) 013105.

- [13] D. H. Whitnum, *Phys. Fluids* 4 (1992) 730; T. V. Liseikina et al, *Phys. Rev. E* 60 (1999) 5991;
E. Esarey, *IP Conference Proceedings* (May 31, 2001) (Volume 569, Issue 1, pp. 473-486).
- [14] A. Chao et al, *Phys. Rev. ST Accel. Beams* 6 (2003) 024201; S. V. Bulanov et al, *Phys. Plasmas* 12 (2005) 073103.

Figure captions

Fig. 1. Typical energy distributions of the electron beam and image of the energy resolved electron beam. A quasi-monoenergetic electron beam with an energy of 19.6 MeV observed at a plasma density equal to $5 \cdot 10^{19} \text{ cm}^{-3}$.

Fig. 2. Images experimentally obtained in a single shot of the spatial (along the vertical axis) and energy (along the horizontal axis) electron distribution with: (a) a single spatial peak and double energy peak; (b) triple spatial peak and triple energy peak.

Fig. 3. Electron energy spectrum versus plasma density. a) experimental data and b) simulation results for $n_e = 4.1 \cdot 10^{19} \text{ cm}^{-3}$ (1); $n_e = 4.7 \cdot 10^{19} \text{ cm}^{-3}$ (2); $n_e = 5 \cdot 10^{19} \text{ cm}^{-3}$ (3); $n_e = 6.6 \cdot 10^{19} \text{ cm}^{-3}$ (4).

Fig. 4. Wake wave seen in the electron density, $n(x; y)$, in the $(x; y)$ plane a); E_z component of the electric field shows the laser pulse modulation b) and E_x component of the electric field of the wake wave, c), along the laser pulse axis, $y = 0$, for $t = 300$.

Fig. 5. Electron phase space: a) plane $(x; p_x)$, b) plane $(y; p_x)$, and c) plane $(x; p_y)$ at $t = 400$. Arrows indicate the electron beam jets. Dashed line indicates a position of the laser pulse front edge.

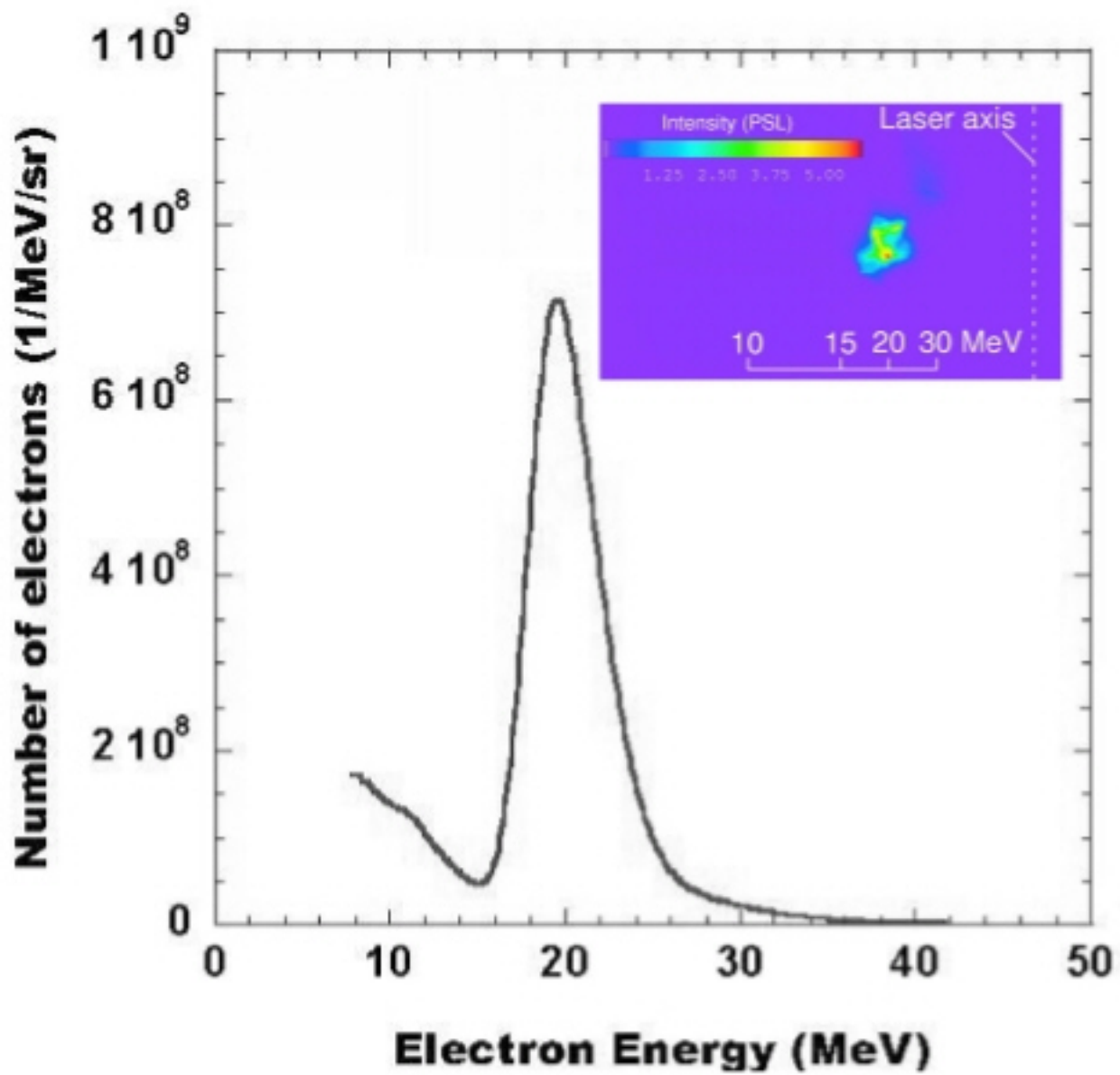


Fig. 1. M MORI

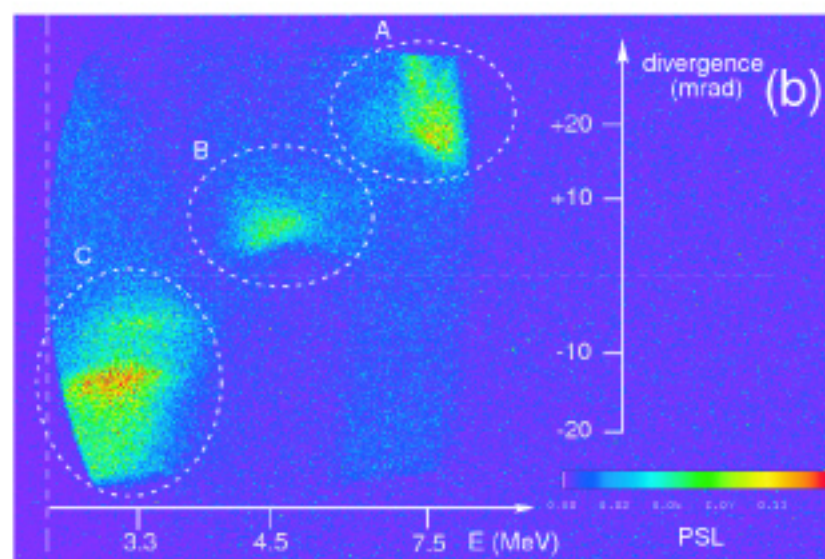
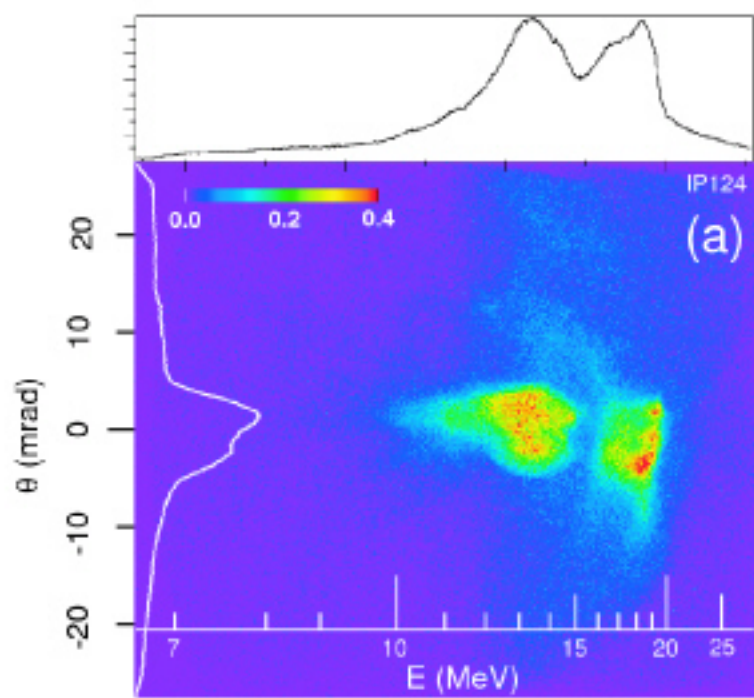


Fig. 2. M MORI

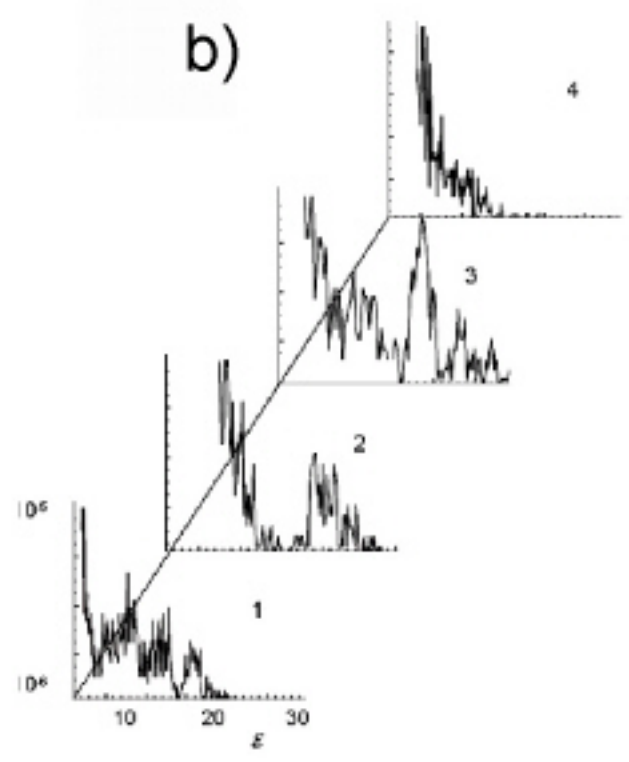
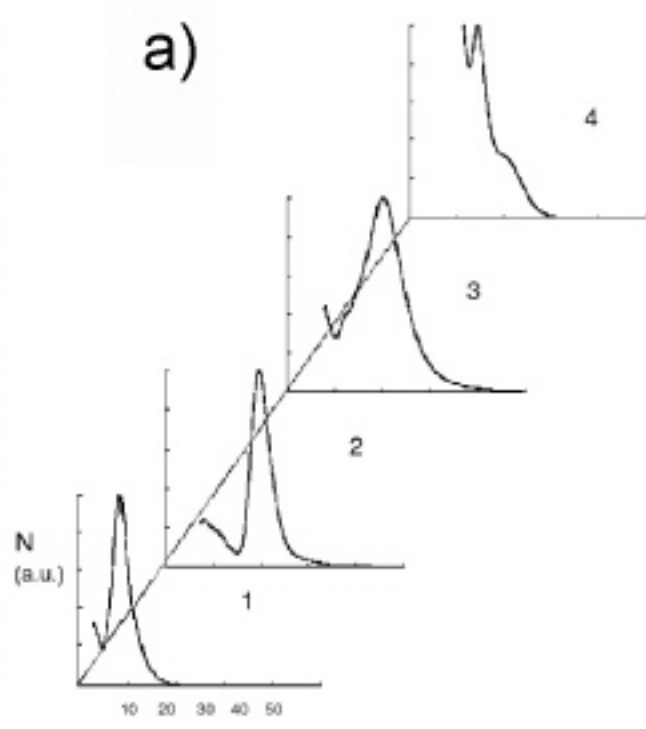


Fig. 3. M MORI

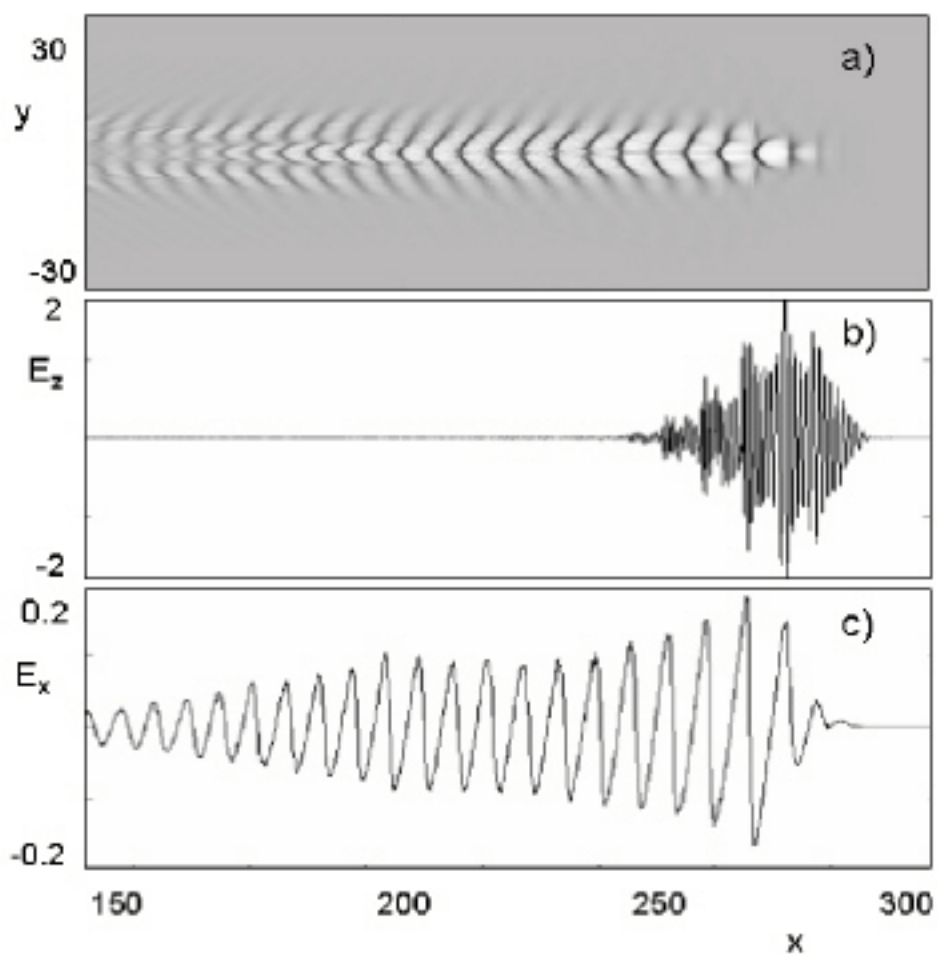


Fig. 4. M MORI

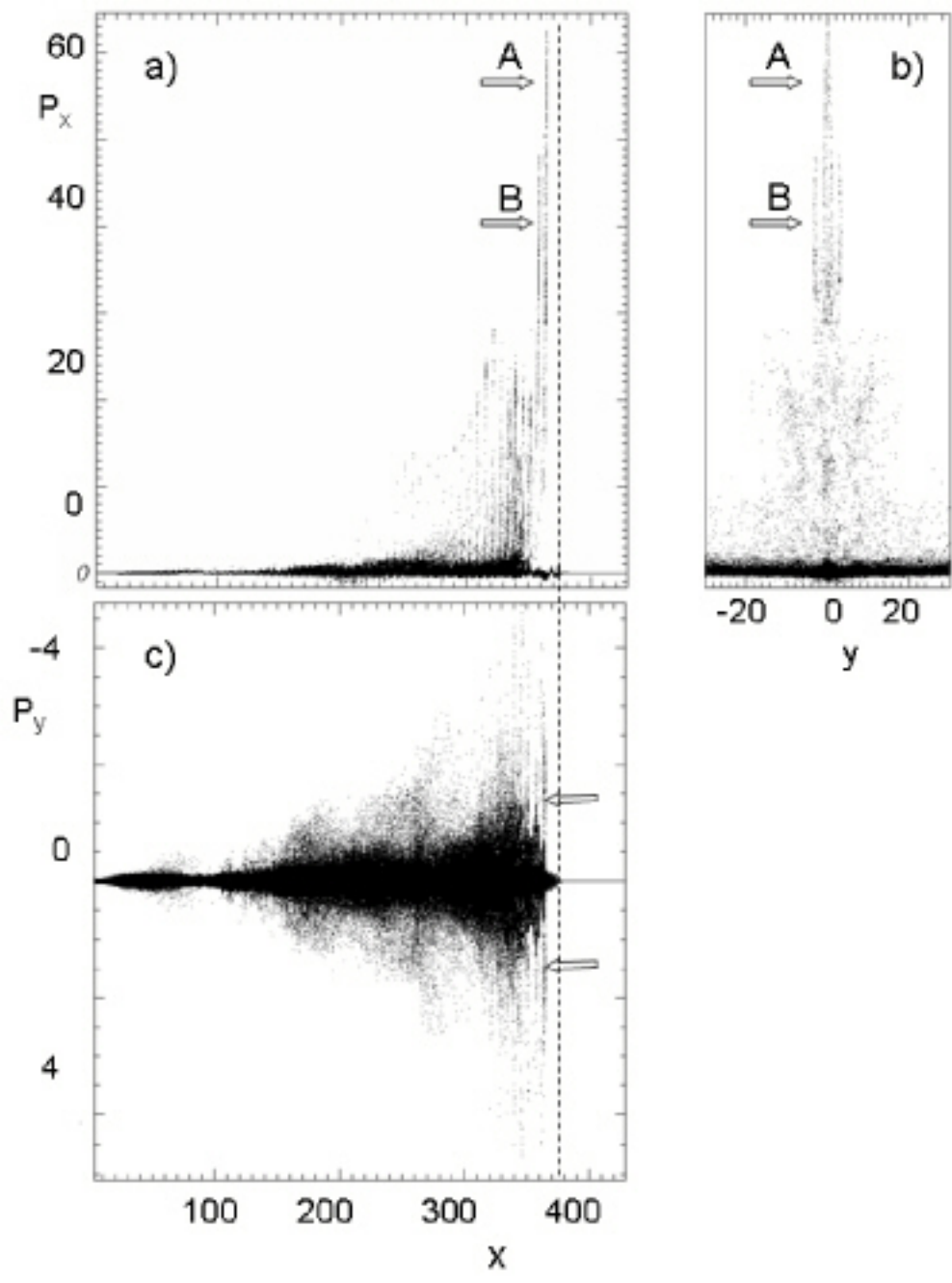


Fig. 5. M MORI